High-Altitude Terminal Control of Anti-Air Missiles With a Terminal Booster and Front Lateral Impulse Thrusters

HA-MIN JEON
TAE YOUNG KANG
Inha University, Incheon, South Korea

JONGHO PARK
Ajou University, Suwon, South Korea

CHANG-KYUNG RYOO
Inha University, Incheon, South Korea

We propose a high-altitude terminal control scheme for anti-air missiles that uses a terminal booster and one-off front lateral impulse thrusters. The terminal booster does not have an actuator, such as thrust vector control, and the front lateral thrusters are cheaper and simpler than the divert attitude control system while providing a faster response than aerodynamic control at high altitudes. The proposed scheme includes a quaternion-based vector-oriented control technique and a firing logic for the front lateral thrusters. The control technique calculates the moment command to track the thrust vector command converted from the acceleration command, which has the advantage that a singularity of Euler angles does not occur. Then, the firing logic using a greedy algorithm selects which unexpired front lateral thrusters to fire so that the direction and magnitude of the moment command can be tracked as closely as possible for the inevitable error due to the discreteness of the front lateral thrusters. Simulations of high-altitude engagement of moving targets were conducted to analyze the performance of the proposed scheme.

Manuscript received 9 March 2023; revised 22 June 2023 and 12 September 2023; accepted 22 December 2023. Date of publication 1 January 2024; date of current version 12 April 2024.

DOI. No. 10.1109/TAES.2023.3348426

Refereeing of this contribution was handled by Y. B. Shtessel.

This work was supported by Theater Defense Research Center funded by Defense Acquisition Program Administration under Grant UD200043CD.

Authors' addresses: Ha-Min Jeon, Tae Young Kang, and Chang-Kyung Ryoo are with Inha University, Incheon 22212, South Korea, E-mail: (haminjeon@naver.com; nantye@naver.com; ckryoo@inha.ac.kr); Jongho Park is with Ajou University, Suwon 16499, South Korea, E-mail: (parkjo05@ajou.ac.kr). *(Corresponding author: Chang-Kyung Ryoo.)*

I. INTRODUCTION

A high-altitude missile defense system is necessary to protect against the increasing threat of ballistic missiles, which has resulted in a corresponding increase in research interest. The hit-to-kill method of using the kinetic energy of an anti-air missile is an effective approach to intercepting a high-speed target. This method requires the missile to have rapid response and maneuverability. However, interception of the target at high altitudes is likely to fail when aerodynamic control is utilized for two main reasons. First, insufficient aerodynamic force and moment are produced at high altitudes because of a lack of dynamic pressure. Second, nonnegligible delay exists on the maneuvering acceleration because of the large turn rate time constant, which represents the speed at which the angle of attack is formed relative to the angular speed [1], [2], [3]. To deal with this problem, the divert attitude control system (DACS), initially developed for spacecraft and satellite systems, has been applied to missile systems. DACS uses four thrusters at the center of gravity and six at the rear end of the missile for trajectory correction or attitude control. However, the complexity of DACS increases production costs. It also increases the weight of the missile, which constrains the launch platform and increases fuel consumption [4]. To overcome these problems, one approach is to equip the missile with a terminal booster that does not need an actuator drive mechanism and cheap front lateral thrusters that offer a faster response than aerodynamic control at high altitudes for attitude control and terminal guidance. PAC-3 ERINT was an early example of a missile equipped with a front lateral thruster [5]. There are three types of lateral thrusters: impulse, open, and shutter. Examples of applications of these types include PAC-3 MSE, S-400, and Aster, respectively [6].

Many researchers have studied continuous lateral thrusters, such as those used in DACS. However, relatively few studies have considered terminal guidance and control using a terminal booster and lateral impulse thrusters under the constraints of one-off, fixed duration, and fixed magnitude. Jeon et al. [7] previously proposed a high-altitude terminal guidance and control loop for a missile equipped with thrust vector control that utilizes the terminal booster and quaternion feedback control technique to track the true proportional navigation (TPN) acceleration command. It is shown that the missile could be guided despite the fixed magnitude of the terminal booster. Zang et al. [8] proposed a firing logic that couples two channels to guarantee guidance accuracy and avoid the possibility of the pulse jet forces being offset. They defined the optimization problem as minimizing the difference between the pitch and yaw force commands and the produced thrust. They showed that the pitch and yaw force commands could be tracked using mixed-integer linear programming. Jitpraphai and Costello [9] proposed a trajectory-tracking flight control system that reduces the dispersion of the expected impact point. The system selects lateral thrusters by considering the position errors of the missile and target, modeling of the lateral

thrusters, the roll rate of the missile, and the burning time of the lateral thrusters. Burchett and Costello [10] proposed a control mechanism of short-duration lateral pulses to reduce the dispersion of the expected impact point for a direct-fire rocket. The dispersion is reduced by calculating the firing time command and selecting the lateral thruster to fire. Their method considers the current roll attitude of the missile rather than the burning time of the lateral thruster, as done by Jitpraphai and Costello [9]. Gao et al. [11] proposed an optimal control method for calculating the firing angle command. The objective function of their optimization problem was to minimize deviations in the impact point considering the vertical and horizontal trajectory correction coefficients, firing delay time, and roll rate of the missile.

We propose a high-altitude terminal control scheme for theater and tactical missile defense that tracks thrust vector commands by using a terminal booster and one-off front lateral impulse thrusters (herewith abbreviated as "front lateral thrusters" for conciseness). The TPN acceleration command is converted into a thrust vector command by using the relative position vector between the missile and the target. Then, front lateral thrusters are selected by a quaternion-based vector-oriented control technique and a firing logic. In previous studies on quaternion feedback control, a singularity of Euler angles could sometimes occur when attitude commands were changed to quaternion commands [12], [13], [14]. To avoid this issue, the introduced technique does not need to calculate the attitude command and does not require feedback on the missile attitude if the command is known in the body coordinate system. In addition, the firing logic is proposed for the front lateral thrusters to track the thrust vector command. Errors are unavoidable because of the fixed duration and magnitude of the force of the front lateral thrusters. The proposed firing logic minimizes these errors by searching the available front lateral thrusters to bind the error quaternion within the predefined threshold. Engagement simulations at high altitudes were conducted to analyze the performance of the proposed scheme [15], [16], [17]. The contributions of this study can be summarized as follows. The proposed scheme can obtain the missile's maneuverability using a terminal booster and one-off front lateral impulse thruster. The overall framework and detailed algorithm of the control system are presented in this article. Moreover, by using multiple front lateral thrusters, it is possible to track both the magnitude and direction of the moment command.

II. MISSILE MODELING

A. Equations of Motion

The engagement geometry between a missile and its target is shown in Fig. 1. $\vec{R}_{TM}$ is the relative range vector between the missile and target, $\vec{\sigma}$ is the line of sight, and $\vec{V}_M$ and $\vec{V}_T$ are the velocity vectors of the missile and target, respectively. $\vec{u}_{\text{tpn}}$ is the TPN acceleration command, $\vec{F}_{MT} = [T \quad 0 \quad 0]^T$ is the thrust of the terminal booster for the missile in the body coordinate system, and $\vec{F}_{LT}$ is the force produced by the front lateral thrusters in the body

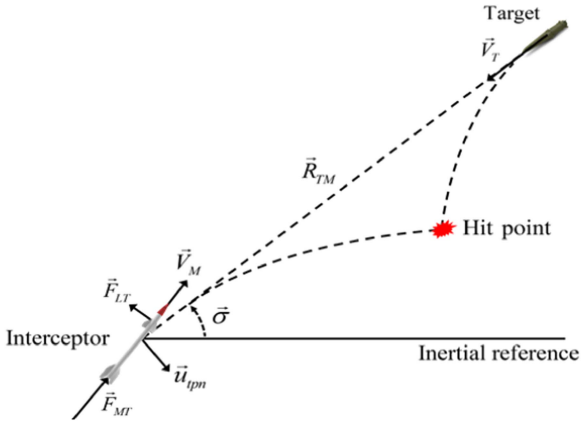

Fig. 1. Missile–target engagement geometry.

coordinate system. In $\vec{F}_{MT}$, T is the magnitude of the thrust of the terminal booster. The translational and rotational motions of the missile are given as follows:

$$m\dot{\vec{v}} + m\left(\vec{\omega} \times \vec{v}\right) - m\,\vec{g} = \vec{F}_A + \vec{F}_{MT} + \sum_{i=1}^{k} \vec{F}_{LT,i} \quad (1)$$

$$J\,\dot{\vec{\omega}} = -\vec{\omega} \times J\vec{\omega} + \vec{M}_A + \sum_{i=1}^{k} \vec{M}_{LT,i} \quad (2)$$

where m is the missile mass, $\vec{v} = [u \quad v \quad w]^T$ is the linear velocity vector of the missile in the body coordinate system, $\vec{\omega} = [p \quad q \quad r]^T$ is the angular velocity vector of the missile, $\vec{g}$ is the gravitational acceleration, J is the inertia matrix, k is the number of front lateral thrusters injected, $\vec{F}_A$ and $\vec{M}_A$ are the aerodynamic force and moment, respectively, and $\vec{M}_{LT}$ is the moment produced by the front lateral thrusters.

B. Modeling of Front Lateral Thrusters

The front lateral thrusters are shown in Fig. 2. We assumed that the lateral thrusters are in front of the missile's center of gravity. Because the space for placing the thrusters can typically be found in front of the center of gravity near the warhead or the guidance and control part. In this case, the missile becomes a minimum phase system. A total of 100 front lateral thrusters are indexed clockwise from the z-axis of the body coordinate system and arranged radially. There are ten rows and ten front lateral thrusters per row. $\vec{F}_{LT,i}$ is the force produced by the ith front lateral thruster, l_i is the axial length from the center of gravity to the ith front lateral thruster, CG_{init} is the initial center of gravity, $\text{CG}_{\text{burnout}}$ is the center of gravity after burning the propellant of the main thruster, and θ_r is the clockwise rotation angle from the z-axis of the body coordinate of the ith front lateral thruster and is described as follows:

$$\vec{M}_{LT,i} = -\|\vec{F}_{LT,i}\| l_i \begin{bmatrix} 0 \\ \cos\theta_r \\ \sin\theta_r \end{bmatrix}. \quad (3)$$

Each front lateral thruster produces a different moment magnitude depending on its moment arm. It is assumed that

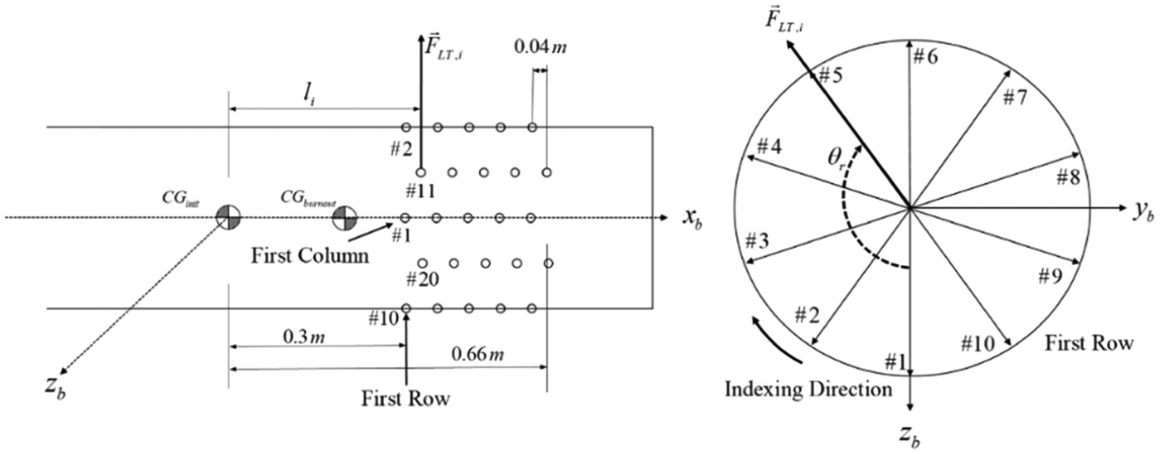

Fig. 2. Configuration of front lateral thrusters.

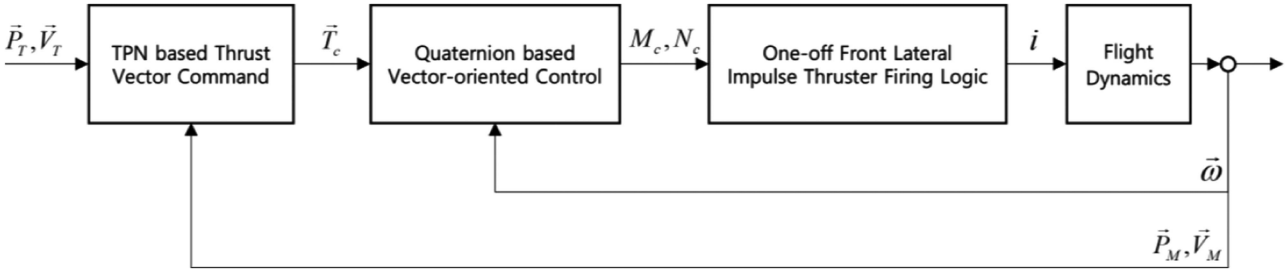

Fig. 3. Schematic diagram of the proposed high-altitude terminal control scheme.

the propellant mass of each front lateral thruster is small, so the change of the center of gravity by the consumption of the front lateral thruster's propellant is neglected. The effect of the difference between each $\vec{F}_{LT}$ on translational motions for a short discrete time is smaller than that of a continuous terminal booster. Note that the front lateral thrusters are arranged radially, so the rolling moment cannot be produced. Furthermore, because the rolling moment caused by aerodynamics is very small at an altitude of theater and tactical missile defense, it is assumed that the missile maintains a constant roll rate, and the performance of the proposed scheme is analyzed according to the initial missile' roll rate [18], [19].

III. PROPOSED HIGH-ALTITUDE TERMINAL CONTROL SCHEME

In the proposed scheme, a missile intercepts a target using 3-D TPN. The rest of the thrust that tracks the guidance command head toward the line of sight. With aerodynamic control, the missile is likely to fail to intercept the target at high altitudes. Thus, we use a terminal booster and front lateral thrusters instead. To track the TPN acceleration command, the proposed scheme controls the missile attitude to change the direction of the terminal booster with a fixed thrust magnitude utilizing the front lateral thrusters. Fig. 3 shows the structure of the proposed scheme, which is a proportional–derivative (PD) type of attitude controller

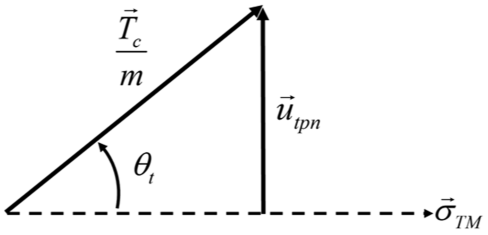

Fig. 4. Definition of the thrust vector command.

loop. Due to little aerodynamic effect at a high altitude, controlling the missile's attitude is a simple second-order problem. Therefore, a PD controller with fixed gain values is enough to control the missile's attitude. First, a thrust vector command ($\vec{T}_c$) is calculated in the reference coordinate system to track the TPN acceleration command. Next, the pitching and yawing moment commands (M_c and N_c) are calculated to track $\vec{T}_c$ by using the error quaternion between the thrust vector command and the longitudinal-axis unit vector of the missile. Finally, the calculated commands and front lateral thruster firing logic are used to select the front lateral thrusters (i) to fire.

A. TPN-Based Thrust Vector Command

In the proposed scheme, the target is intercepted by tracking the thrust vector command converted from the TPN acceleration command. Fig. 4 defines the thrust vector

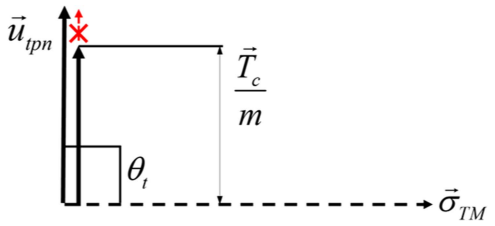

Fig. 5. Saturation of the thrust vector command.

command. The conversion of the thrust vector command is divided into two steps. First, the TPN acceleration command in the reference coordinate system is calculated by using the position and velocity of the missile and target. The 3-D TPN acceleration command is given by

$$\vec{u}_{\text{tpn}} = NV_c\dot{\vec{\sigma}}_{TM} \tag{4}$$

where N is the navigation constant and V_c is the closing velocity. $\dot{\vec{\sigma}}_{TM}$ is the line of sight rate and is represented as follows:

$$\dot{\vec{\sigma}}_{TM} = \frac{\vec{R}_{TM} \times \vec{V}_{TM}}{||\vec{R}_{TM}||^2} \tag{5}$$

where $\vec{V}_{TM}$ is the relative velocity vector between the missile and target. $\vec{R}_{TM}$ and $\vec{V}_{TM}$ are given as follows:

$$\vec{R}_{TM} = \vec{P}_T - \vec{P}_M \tag{6}$$

$$\vec{V}_{TM} = \vec{V}_T - \vec{V}_M \tag{7}$$

where $\vec{P}_T$ and $\vec{P}_M$ are the position vectors of the missile and target, respectively. Next, the calculated acceleration command and the relative range vector between the missile and target are used to obtain the thrust vector command

$$\vec{T}_c = m\vec{u}_{\text{tpn}} + T\cos\theta_t \frac{\vec{R}_{TM}}{\|\vec{R}_{TM}\|} \tag{8}$$

θ_t is the included angle of the triangle comprising the acceleration command and thrust vector command and is given by

$$\theta_t = \sin^{-1}\frac{\|m\vec{u}_{\text{tpn}}\|}{T}. \tag{9}$$

If the magnitude of the force required to track the acceleration command is greater than the magnitude of the thrust of the terminal booster, then the acceleration command cannot be tracked, as shown in Fig. 5. Therefore, the saturation condition of the acceleration command can be formulated as follows:

$$\text{if } \|m\vec{u}_{\text{tpn}}\| \geq T,\ \vec{u}_{\text{tpn}} = \frac{T\vec{u}_{\text{tpn}}}{\|m\vec{u}_{\text{tpn}}\|}. \tag{10}$$

B. Quaternion-Based Vector-Oriented Control

In the proposed scheme, guidance commands are tracked by controlling the missile attitude. We utilize a quaternion-based vector-oriented control for the missile attitude that calculates an error quaternion by using the relationship between two vectors, not two quaternions.

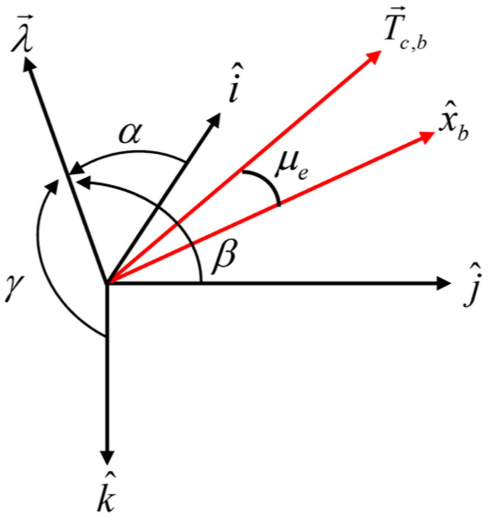

Fig. 6. Definition of the error quaternion.

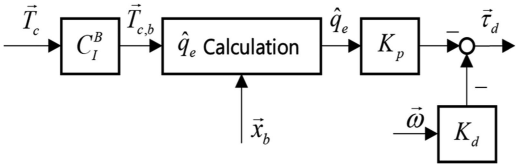

Fig. 7. Quaternion-based vector-oriented control.

The error quaternion between the thrust vector command and the longitudinal-axis unit vector of the missile ($\hat{x}_b$) can be decreased by using this technique. Fig. 6 defines the error quaternion. $\vec{\lambda}$ and μ_e are the Euler axis and rotation angle of the error quaternion, respectively. The angle components α, β, and γ of $\vec{\lambda}$ signify the direction cosine angles and define the direction of $\vec{\lambda}$. $\hat{i}$, $\hat{j}$, and $\hat{k}$ represent the unit vectors in the reference coordinate system. To decrease the error quaternion, the inner loop of the proposed scheme calculates the moment command that is required to direct the longitudinal-axis unit vector of the missile to the thrust vector command, as shown in Fig. 7. With this method, there is no need to convert the thrust vector command into an attitude command, so a singularity does not occur. Moreover, there is no need to require feedback on the missile attitude if the thrust vector command is known in the body coordinate system. The calculation of the moment commands is divided into two steps. First, $\vec{\lambda}$ and μ_e are obtained from the definitions of the dot product and cross product as follows:

$$\mu_e = \cos^{-1}\frac{\vec{T}_{c,b}\cdot\hat{x}_b}{\|\vec{T}_{c,b}\|\|\hat{x}_b\|} \tag{11}$$

$$\begin{aligned}\vec{\lambda} &= \cos\alpha\hat{i} + \cos\beta\hat{j} + \cos\gamma\hat{k} \\ &= \frac{q_{1t}}{\sqrt{q_{1t}^2+q_{2t}^2+q_{3t}^2}}\hat{i} \\ &\quad + \frac{q_{2t}}{\sqrt{q_{1t}^2+q_{2t}^2+q_{3t}^2}}\hat{j} + \frac{q_{3t}}{\sqrt{q_{1t}^2+q_{2t}^2+q_{3t}^2}}\hat{k}\end{aligned} \tag{12}$$

$$\vec{q}_t = \begin{bmatrix} q_{1t} & q_{2t} & q_{3t} \end{bmatrix}^T = \frac{\vec{T}_{c,b} \times \hat{x}_b}{\|\vec{T}_{c,b}\| \|\hat{x}_b\|} \tag{13}$$

where $\vec{T}_{c,b}$ is the thrust vector command in the body coordinate system. Next, the moment command is calculated by using μ_e, β, γ and q, r

$$\begin{aligned} M_c &= -K_p \sin\frac{\mu_e}{2}\cos\beta - K_d q \\ N_c &= -K_p \sin\frac{\mu_e}{2}\cos\gamma - K_d r \end{aligned} \tag{14}$$

where K_p and K_d are the proportional gain and differential gain, respectively. Due to the one-off injection of the front lateral thrusters, a parameter study is performed via simulation instead of the root locus analysis to select K_p and K_d by examining time-domain specifications, such as rise time and settling time.

C. Front Lateral Thruster Firing Logic

The front lateral thruster considered in this study can produce a relatively large force in a short period.

However, it cannot produce continuous moments due to the discrete front lateral thruster arrangement and fixed injection time.

A front lateral thruster firing logic using a greedy algorithm is proposed to select a front lateral thruster combination that can produce moments as close as possible to the calculated command. The greedy algorithm is used to solve the optimization problem. At each step, it makes the best choice, although it is not a global solution to the corresponding optimization problem. Furthermore, it is known to be simple, intuitive, easy to implement, and faster than other algorithms, such as dynamic programming and complete enumeration [20]. Table I summarizes the greedy algorithm of the proposed firing logic for selecting which front lateral thrusters to be fired.

In Table I, $N_{\max}$ is the maximum number of front lateral thrusters to be fired at once, i_u is the front lateral thrusters currently available, i is the front lateral thruster index to be fired, N_i is the total number of front lateral thrusters to be fired, and N_p is the total number of front lateral thrusters. The process for selecting front lateral thrusters is given as follows.

1) Select the front lateral thrusters that can produce the moment as close as possible to the moment command.
2) A new moment command is calculated by subtracting the moment produced by the selected front lateral thrusters from the current moment command.
3) Save the selected front lateral thrusters.
4) Determine the algorithm termination condition by using the moment command before subtraction, the new moment command, and $N_{\max}$.
5) Repeat #1–#4, and if the termination condition is satisfied, return the finally selected front lateral thruster combination (i), the number of front lateral thrusters to fire ($N_{\max}$), and the unfired front lateral thrusters (i_u).

TABLE I
Pseudocode of the Front Lateral Thruster Firing Logic Using a Greedy Algorithm

Design Parameters: N_{max}; N_p;
Input: M_c; N_c; i_u;
Output: i; i_u; N_i
Begin

Obtain $\vec{P}_T$, $\vec{P}_M$, $\vec{V}_T$, $\vec{V}_M$, $\vec{w}$;
Compute $\vec{u}_{tpn}$ using (5)–(8);
if (11) is true **then**
Saturate $\vec{u}_{tpn}$;
end
Compute $\vec{T}_c$ using (9);
Obtain C_I^B;
Compute $\vec{T}_{c,b}$ using C_I^B and $\vec{T}_c$;
Compute M_c, N_c using (12)-(15);
idx = 1;
l_{save} = [ ];
$M_{c,after}$ = M_c;
$N_{c,after}$ = N_c;

While(true)
$l = i_u^* =$
$\min_{i_u} \sqrt{(M_{c,after} - M_{i_u})^2 + (N_{c,after} - N_{i_u})^2}$;
$M_{c,prev}$ = $M_{c,after}$;
$N_{c,prev}$ = $N_{c,after}$;
$M_{c,after}$ = $M_{c,after} - M_l$;
$N_{c,after}$ = $N_{c,after} - N_l$;
$l_{save}(idx)$ = l;

if $\sqrt{M_{c,after}^2 - N_{c,after}^2} > \sqrt{M_{c,prev}^2 - N_{c,prev}^2}$
or $idx > N_{max}$ is true **then**
$l_{save}(end)$ = [ ];
i = l_{save};
N_i = idx - 1;
break;
end

Update i_u (= Remove l at i_u);
idx = idx + 1;
end

end

To reduce the consumption of front lateral thrusters, a dead zone is set where the front lateral thrusters are fired if the rotation angle of the error quaternion is greater than the threshold value ($\mu_{e,\text{thres}}$)

$$\|\mu_e\| \geq \mu_{e,\text{thres}} \rightarrow \text{Thrusters ON} \tag{15}$$
$$\|\mu_e\| < \mu_{e,\text{thres}} \rightarrow \text{Thrusters OFF.} \tag{16}$$

TABLE II
Initial Missile Conditions

Parameter	Initial value	Units
$\vec{P}_{M,I}$	0 / 0 / -60	km
u / v / w	1000 / 0 / 0	m/s
p / q / r	60 / 0 / 0	°/s
m	74	kg
m_p	30	kg
$\dot{m}_p$	−2.4	kg/s
I_{xx} / I_{yy} / I_{zz}	0.3 / 24.8 / 24.8	kg m^2
$\dot{I}_{xx}$ / $\dot{I}_{yy}$ / $\dot{I}_{zz}$	−0.01 / −0.81 / −0.81	kg m^2
K_p / K_d	7200 / 1200	-
I_{sp}	250	s
$\|\vec{F}_{LT}\|$	3000	N
N_p	100	pcs
N_{max}	4	pcs
$\mu_{e,thres}$	6	°
N	3	-
Δt / t_b	0.0001 / 0.01	s
Relative range	20	km
σ_θ / σ_ψ	30 / 0	°
ψ	0	°
Target heading angle	180	°
Target flight path angle	−30	°
Target velocity	2000	m/s

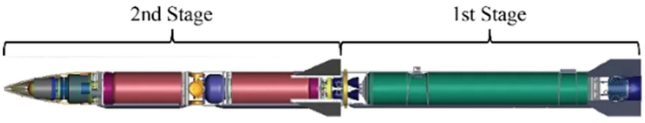

Fig. 8. NCADE missile configuration [22].

IV. NUMERICAL SIMULATIONS

Engagement simulations against nonmaneuvering reentry vehicles were conducted, and the capture region was investigated to analyze the performance of the proposed scheme. Table II presents the common initial conditions for the simulation. m_p is the total propellant mass of the missile, and $\dot{m}_p$ is the change in the total propellant mass. I_{xx}, I_{yy}, and I_{zz} are the moments of inertia of the missile with respect to the x, y, and z axes, respectively, of the body coordinate system, and $\dot{I}_{xx}$, $\dot{I}_{yy}$, and $\dot{I}_{zz}$ are the corresponding changes in the moments of inertia. Δt is the simulation step time, t_b is the duration of the impulses, and σ_θ and σ_ψ are the initial pitch and yaw line-of-sight angles.

Fig. 8 shows the configuration of the network-centric airborne defense element (NCADE) missile.

We adopted the properties of the second stage of the NCADE missile for the simulation [21], [22]. The main specifications of an NCADE missile are as follows: m = 74 kg, I_{xx} = 0.3 kg·m^2, I_{yy} = 24.8 kg·m^2, and I_{zz} = 24.8 kg·m^2. The moments of inertia were calculated by assuming that the missile shape is a cylinder. In addition,

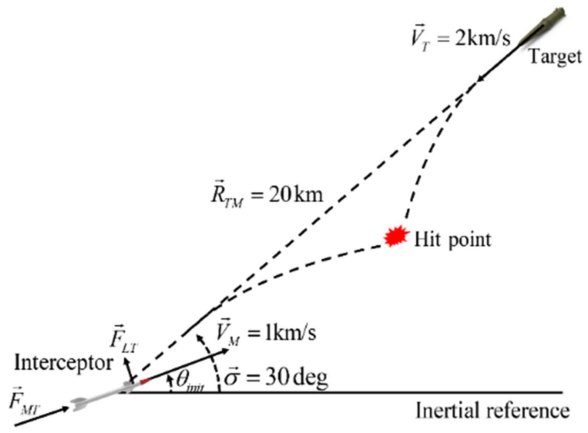

Fig. 9. Engagement geometry for a single-run simulation (Case 1).

m_p = 45 kg, $\dot{m}_p$ = 2.4 kg/s, and the specific impulse was I_{sp} = 250 s. The aerodynamic coefficients of the NCADE are calculated using the missile DATCOM program [23], and it is assumed that the missile is stabilized after midcourse guidance. The guidance command is calculated every 0.1 s. The mass, the moment of inertia, and the length from the missile's nose to the center of gravity are set to decrease linearly in terms of the amount of the terminal booster's propellant. Note that the front lateral thrusters are generally solid-fuel motors, and the thrust is usually prone to deviation. Therefore, in every simulation, thrust deviations are applied by adding a random number within 1% of the front lateral thruster's thrust magnitude using continuous uniform distribution to each front lateral thruster's thrust magnitude. Finally, three degrees-of-freedom equations of motion were used for the ballistic target.

A. Case 1

In Case 1, the single-run simulation results were compared and analyzed according to the initial pitch attitude of the missile (θ_{init}). In addition to the initial conditions, as given in Table II, the following initial pitch attitudes were considered: 17.5°, 20°, 22.5°, 25°, and 27.5°. Fig. 9 shows the engagement geometry. Note that $\vec{V}_M$ and $\vec{F}_{MT}$ are aligned with x_b. Fig. 10 shows the trajectories of the missile and target, and the missile heads toward the target in all cases. At initial pitch attitudes of 17.5°, 20°, 22.5°, 25°, and 27.5°, the final miss distances were 0.0481 m, 0.0482 m, 0.0595 m, 0.0414 m, and 0.0269 m, respectively, which satisfy the hit-to-kill condition.

Fig. 11 shows the magnitude of the missile velocity. The flight speed of the missile was increased by the terminal booster. The flight speed was faster at an initial pitch attitude of 27.5° than at 17.5°, 20°, 22.5°, and 25° for the same initial relative range between the missile and target. Fig. 12 shows the quaternion of the missile. An initial pitch attitude of 27.5° resulted in the smallest change in the missile attitude and the shortest flight time. Fig. 13 shows the error quaternion of the missile. And Fig. 14 shows the angular velocity of the missile. The changes in the angular velocity were discontinuous because of the discrete actions of the

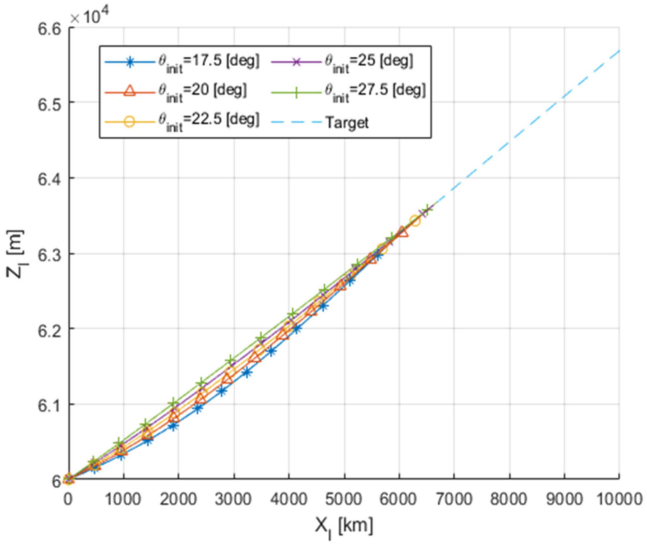

Fig. 10. Trajectories of the missile and target (Case 1).

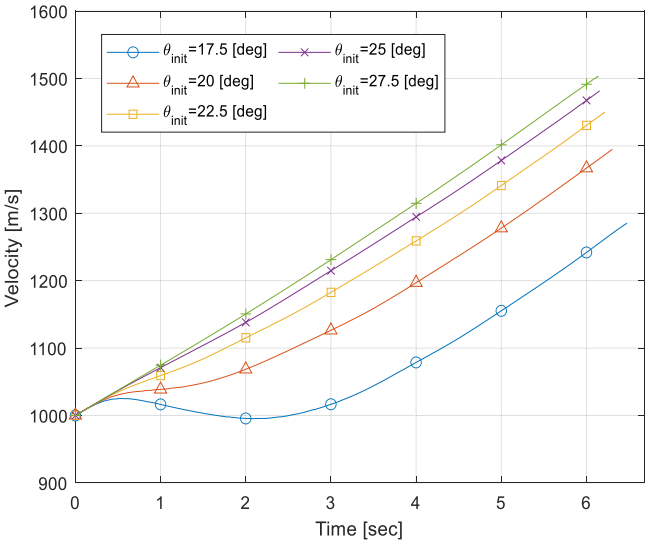

Fig. 11. Magnitude of the missile velocity (Case 1).

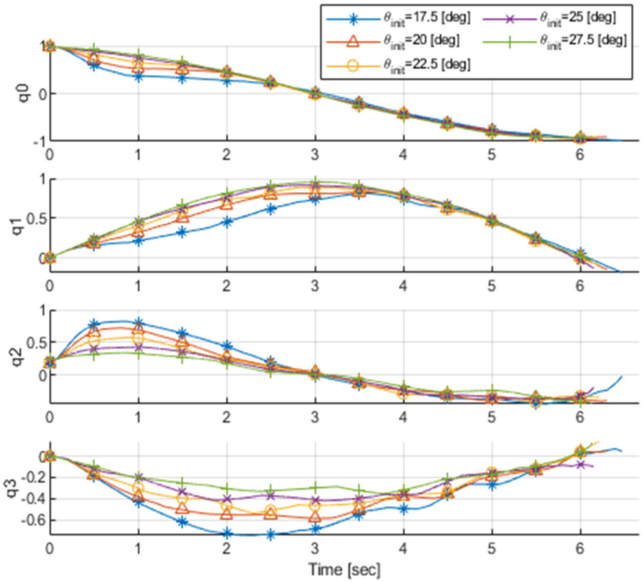

Fig. 12. Quaternion of the missile (Case 1).

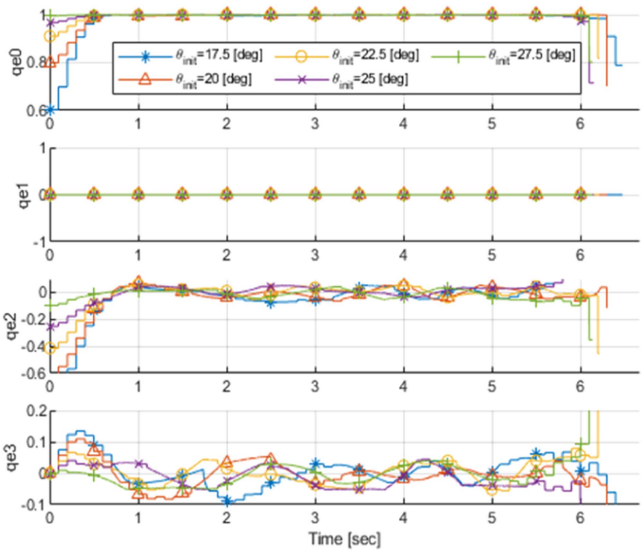

Fig. 13. Error quaternion of the missile (Case 1).

front lateral thrusters. The changes in angular velocity were smaller at an initial pitch attitude of 27.5° than at 17.5°, 20°, 22.5°, and 25°. Fig. 15 shows the injected front lateral thruster index and the change in the error quaternion. The front lateral thrusters were not used redundantly. Initial pitch attitudes of 17.5°, 20°, 22.5°, 25°, and 27.5° resulted in the use of 62, 39, 46, 37, and 30 front lateral thrusters, respectively. Fig. 16 shows the thrust produced by each fired front lateral thruster when $\theta_{\text{init}} = 25°$, and each front lateral thruster produces a different magnitude of the thrust by the simulation's assumption. Figs. 17 and 18 show the aerodynamic force and moment, and Fig. 19 shows the pitching moment, yawing moment, and the magnitude of the moment produced by the front lateral thrusters when $\theta_{\text{init}} = 25°$. In Fig. 17, the aerodynamic forces produced from the fuselage and fin of the missile are dominated in the x–z plane of the reference coordinate system by the engagement condition. On the other hand, Figs. 18 and 19 show that the aerodynamic moment is small compared with the moment produced by the front lateral thrusters. Fig. 19 shows that moment command is within the levels that can be produced using multiple thrusters. Fig. 20 shows the computing time required to select a front lateral thruster combination when $\theta_{\text{init}} = 25°$, and the mean computing time is 0.409 ms. Figs. 13 and 15 show that q_{e0} converged to 1 because the rotation angle of the error quaternion (μ_e) converged to zero in about 1 s. However, the rotation angle of the error quaternion was occasionally outside the dead zone, which is why the front lateral thrusters were fired even after convergence. The number of front lateral thruster injections increased with an increasing difference between the initial line of sight and the missile attitude. This means that more maneuvers and a greater change in the missile attitude were required, which increased the rotation angle

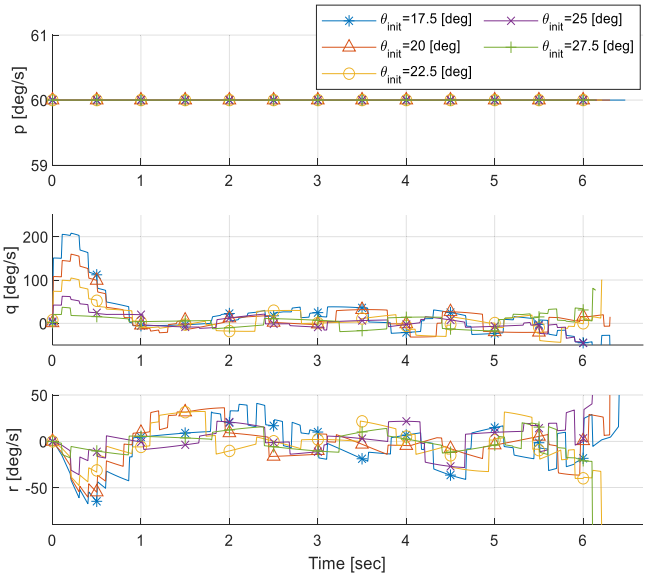

Fig. 14. Angular velocity of the missile (Case 1).

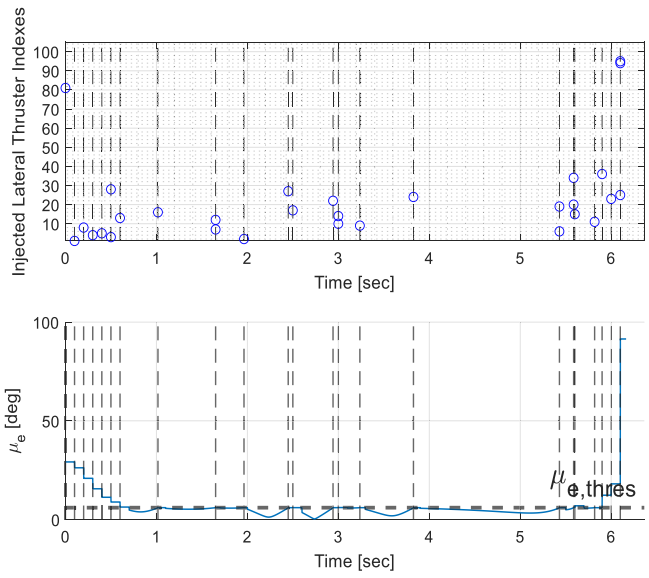

Fig. 15. Injected front lateral thruster index (Case 1, $\theta_{\text{init}} = 25°$).

of the error quaternion. Therefore, the rotation angle was often outside the dead zone when a front lateral thruster was injected, which increased the number of injections. In addition, the large change in the missile attitude resulted in a smaller increase in the missile speed and a longer flight time.

B. Case 2

In Case 2, the capture regions were compared and analyzed according to the initial pitch/yaw attitudes of the missile ($\theta_{\text{init}}/\psi_{\text{init}}$), the initial relative range between the missile and target, the missile's roll rate, and $N_{\max}$. The uncertainty of aerodynamic coefficients and the thrust magnitude of the thruster are only considered. We use the miss distance of 0.5 m for calculating the capture region. Figs. 21–23 show the capture region, and Fig. 24 shows the

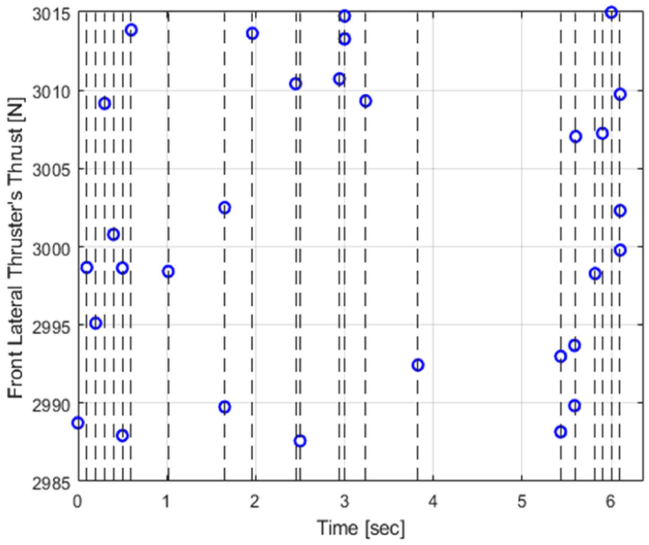

Fig. 16. Thrust produced by each fired front lateral thruster (Case 1, $\theta_{\text{init}} = 25°$).

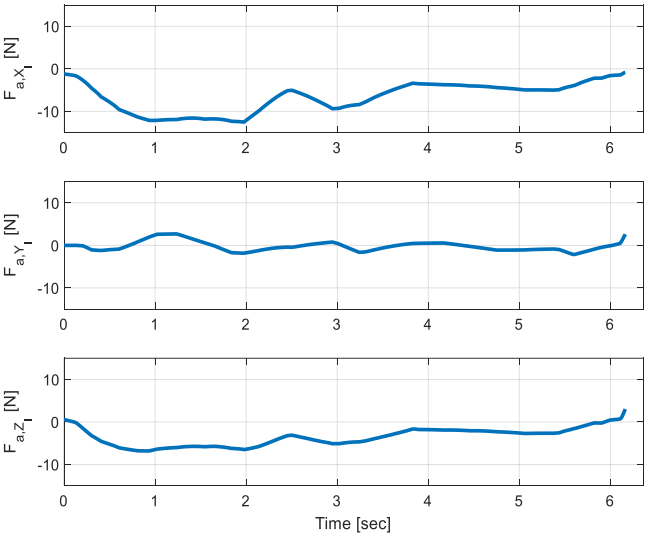

Fig. 17. Aerodynamic force (Case 1, $\theta_{\text{init}} = 25°$).

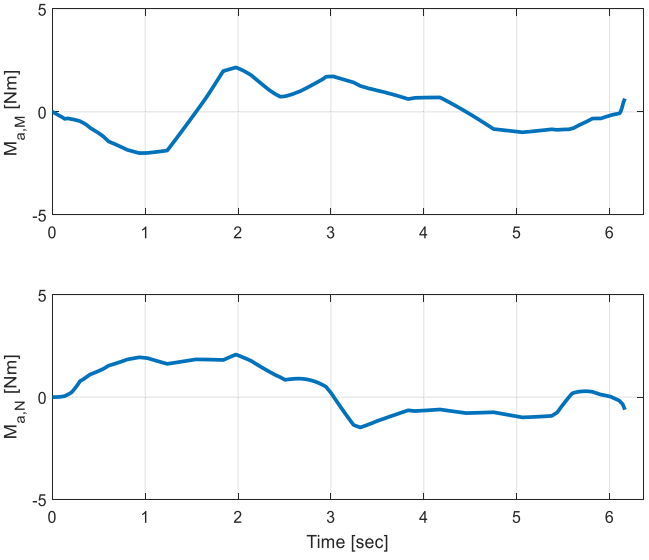

Fig. 18. Aerodynamic moment (Case 1, $\theta_{\text{init}} = 25°$).

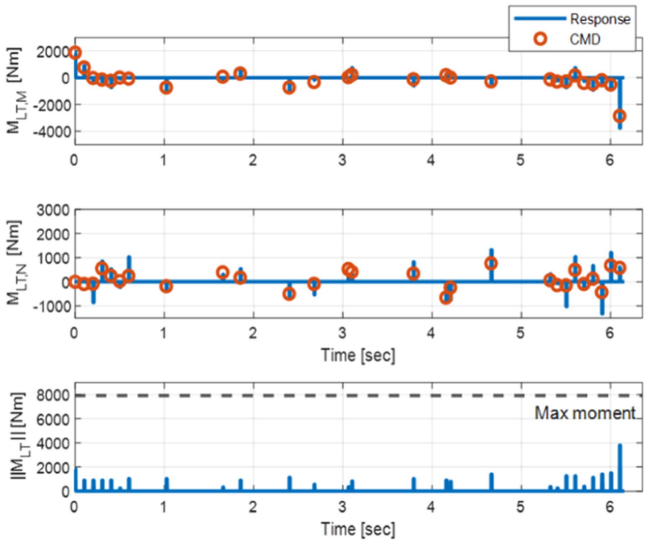

Fig. 19. Moment produced by front lateral thrusters (Case 1, $\theta_{\text{init}} = 25°$).

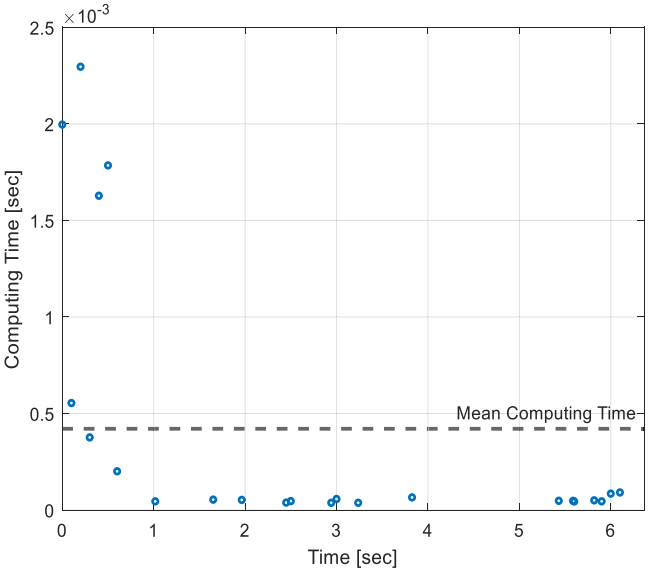

Fig. 20. Computing time required to select front lateral thruster combination (Case 1, $\theta_{\text{init}} = 25°$).

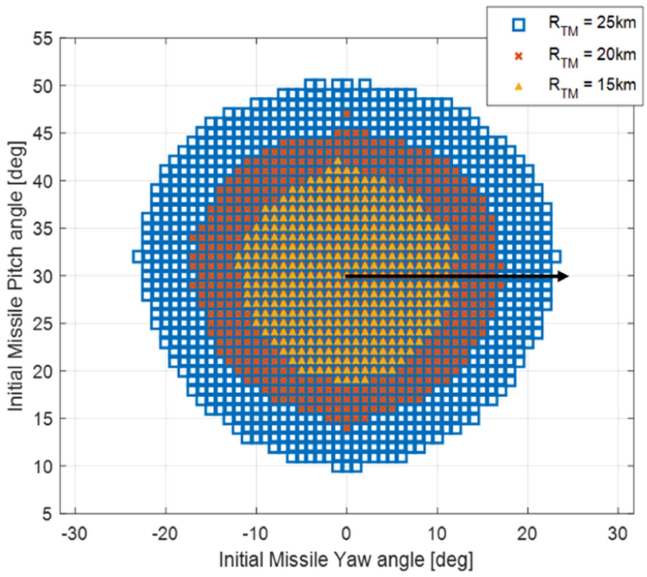

Fig. 21. Capture region (Case 2-1).

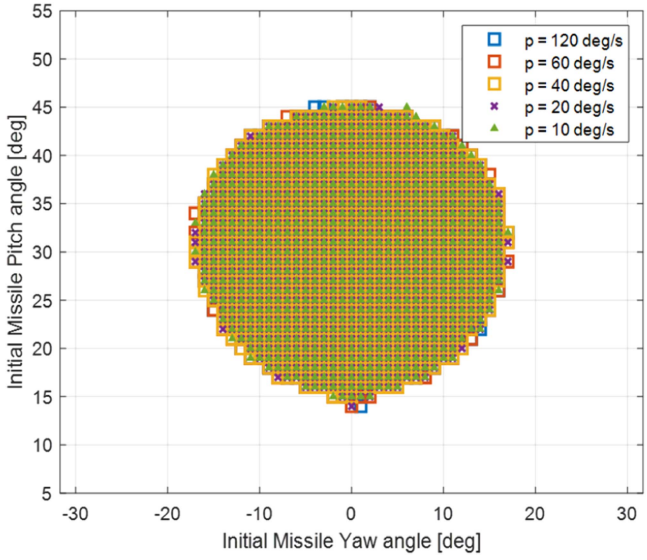

Fig. 22. Capture region (Case 2-2).

number of front lateral thrusters injected according to the ψ_{init} in the direction of the arrow in Fig. 21 when $\theta_{\text{init}} = 30°$.

1) *Case 2-1:* In addition to the initial conditions, as given in Table II, the following initial relative ranges between the missile and target were considered for computing the capture region of the missile: 15 km, 20 km, and 25 km. At initial relative ranges of 15 km, 20 km, and 25 km, successful interceptions had 48.03, 47.98, and 52.09 front lateral thruster injections, respectively, on average. Fig. 21 shows that the capture region was the largest with the longest initial relative range because the missile had enough time for interception. Fig. 24 shows that the number of front lateral thruster injections increased as the difference between the initial line of sight and initial pitch/yaw attitudes of the missile increased for the same reason as in Case 1.

2) *Case 2-2:* In addition to the initial conditions, as given in Table II, the following initial missile roll rates were considered to compute the capture region of the missile: 10°/s, 20°/s, 40°/s, 60°/s, and 120°/s. At the initial missile roll rate of 10°/s, 20°/s, 40°/s, 60°/s, and 120°/s, successful interceptions had 49.31, 48.72, 47.76, 47.98, and 48.64 front lateral thruster injections, respectively, on average. Fig. 22 shows that the capture region according to the missile roll rate was almost similar to each other and that the algorithm works well even when the missile's roll rate is slow.

3) *Case 2-3:* In addition to the initial conditions, as given in Table II, N_{max} were considered to compute the capture region of the missile: 2, 4, and 6. At N_{max} of 2, 4, and 6, successful interceptions had 47.98, 47.65, and 45.13 front lateral thruster injections, respectively, on average. Fig. 23 shows that the capture region according to N_{max} was almost similar to each other.

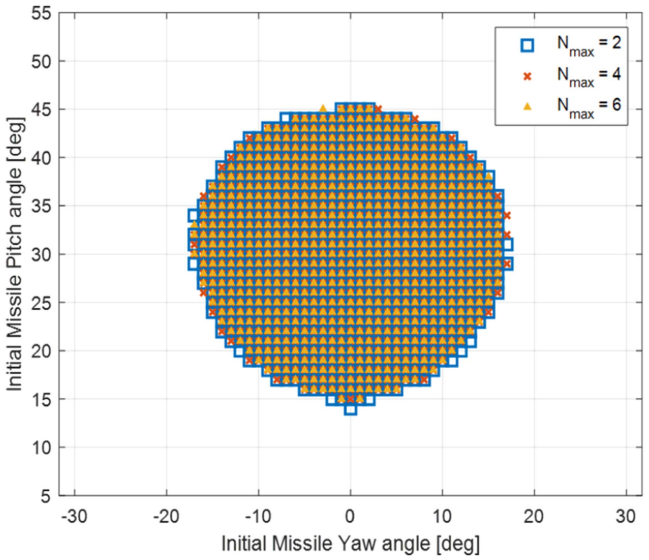

Fig. 23. Capture region (Case 2-3).

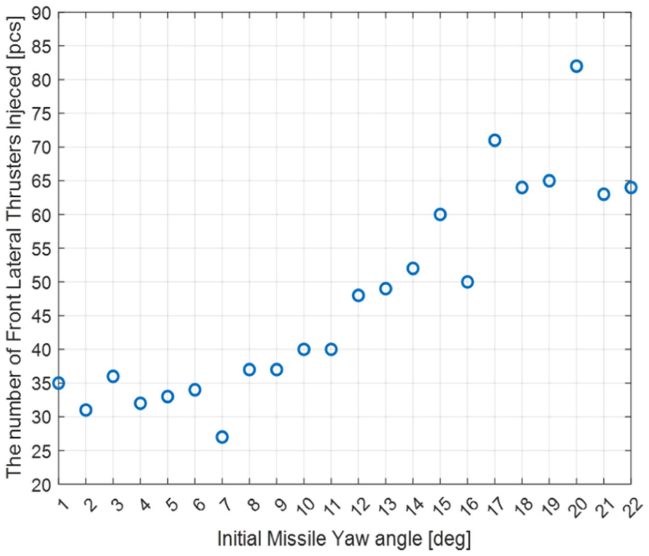

Fig. 24. Number of front lateral thruster injections (Case 2-1, $\theta_{\text{init}} = 30°$).

V. DISCUSSION AND CONCLUSION

We proposed a high-altitude terminal control scheme for anti-air missiles equipped with a terminal booster and front lateral thrusters. The terminal booster does not include an actuator drive mechanism, and the front lateral thrusters are one-off and the impulse type. Engagement simulations were conducted to analyze the effects of the initial attitude, initial relative range, roll rate, and the maximum number of front lateral thrusters to fire at once on the interception performance. The simulation results showed that the terminal booster and front lateral thrusters could provide terminal guidance at high altitudes where aerodynamic control is difficult. In addition, the guidance could be achieved even with the fixed magnitude of the terminal booster with the help of the front lateral thrusters.

The contributions of this study can be summarized as follows. First, the proposed scheme seeks front lateral thrusters by considering pitching and yawing moment commands instead of position errors, as considered in the previous studies [8], [9]. Thus, it can track commonly used guidance commands, such as proportional or optimal guidance. Moreover, using multiple front lateral thrusters allows not only the direction of the moment command but also the magnitude of the moment command to be tracked. With the quaternion-based vector-oriented control technique, there is no need for feedback on the missile attitude if the guidance command is provided in the body coordinate system. Singularities are a well-known problem with Euler angles, but the proposed scheme eliminates this issue. Furthermore, instead of the firing command time being calculated based on the current time, the proposed scheme can immediately determine the front lateral thrusters that need to be fired. Finally, the proposed scheme can obtain the maneuverability of the missile when using a terminal booster with a fixed magnitude based on the solid rocket motor thrust. Future work will involve extending the proposed scheme to obtain the optimal solution and conducting a parametric study.

REFERENCES

[1] C.-H. Lee, T.-H. Kim, and B.-E. Jun, "Nonlinear acceleration controller design for DACS type kill vehicle," *J. Korean Soc. Propul. Engineers*, vol. 19, no. 3, pp. 54–64, 2015.

[2] S. Ann, S. Lee, and Y. Kim, "Intercept point prediction for midcourse guidance of anti-ballistic missile," in *Proc. 26th Mediterranean Conf. Control Autom.*, 2018, pp. 1–9.

[3] H. R. Park, "The ballistic missile defense construction strategies of South Korea and Japan: Self-reliance versus cooperation with the US," *J. Int. Area Stud.*, vol. 25, no. 2, pp. 87–105, 2018.

[4] R. Głębocki and M. Jacewicz, "Parametric study of guidance of a 160-mm projectile steered with lateral thrusters," *Aerospace*, vol. 7, no. 5, 2020, Art. no. 61.

[5] S. W. Lang, "PAC-3: The evolution of a system from concept for deployment," ARMY Space Missile Defense Comm. Corp., Huntsville, AL, USA, 2011.

[6] W.-H. Kim, B.-E. Lee, S.-H. Koo, and W.-B. Lee, "Study on the technical trend of a pulse separation device with thermal barrier type," in *Proc. Korean Soc. Propul. Engineers Conf.*, 2010, pp. 225–228.

[7] H.-M. Jeon, J.-H. Park, and C. Ryoo, "High-altitude terminal guidance and control loop design using thrust vector control," *J. Korean Soc. Aeronaut. Space Sci.*, vol. 50, no. 6, pp. 393–400, 2022.

[8] Y. Zang, B. Yang, X. Huo, and S. Chen, "Firing logic design for ACS of missile with pulse jets," in *Proc. Chin. Control Des. Conf.*, 2016, pp. 5596–5601.

[9] T. Jitpraphai and M. Costello, "Dispersion reduction of a direct fire rocket using lateral pulse jets," *J. Spacecraft Rockets*, vol. 38, no. 6, pp. 929–936, 2001.

[10] B. Burchett and M. Costello, "Model predictive lateral pulse jet control of an atmospheric rocket," *J. Guid., Control, Dyn.*, vol. 25, no. 5, pp. 860–867, 2002.

[11] M. Gao, Y. Zhang, and S. Yang, "Firing control optimization of impulse thrusters for trajectory correction projectiles," *Int. J. Aerosp. Eng.*, vol. 2015, no. 2, 2015, Art. no. 781472.

[12] B. Wie, H. Weiss, and A. Arapostathis, "Quarternion feedback regulator for spacecraft eigenaxis rotation," *J. Guid., Control, Dyn.*, vol. 12, no. 3, pp. 375–380, 1989.

[13] S.-J. Kim, C.-K. Ryoo, and K. Choi, "Robust attitude control via quaternion feedback linearization," in *Proc. SICE Annu. Conf.*, 2007, pp. 2234–2239.

[14] C. Song, S.-J. Kim, S.-H. Kim, and H. S. Nam, "Robust control of the missile attitude based on quaternion feedback," *Control Eng. Pract.*, vol. 14, no. 7, pp. 811–818, 2006.
[15] P. Zarchan, *Tactical and Strategic Missile Guidance*. New York, NY, USA: McGraw-Hill, 2007, pp. 13–34.
[16] G. M. Siouris, *Missile Guidance and Control System*. New York, NY, USA: Springer, 2006, pp. 155–266.
[17] B. L. Stevens, F. L. Lewis, and E. N. Johnson, *Aircraft Control and Simulation: Dynamics, Controls Design, and Autonomous Systems*. Hoboken, NJ, USA: Wiley, 2015, pp. 1–58.
[18] S. G. Park and K. H. Lee, "A study on the establishment of capability-based multi-layered missile defense system considering MD in U.S.," *J. Korea Inst. Mil. Sci. Technol.*, vol. 3, no. 1, pp. 46–55, 2020.
[19] S. Yunn and S. Kim, "A study on the optimal allocation of Korea air and missile defense system using a genetic algorithm," *J. Korea Inst. Mil. Sci. Technol.*, vol. 18, no. 6, pp. 797–807, 2015.
[20] G. L. Nemhauser, L. A. Wolsey, and M. L. Fisher, "An analysis of approximations for maximizing submodular set functions—I," *Math. Program.*, vol. 14, no. 1, pp. 265–294, 1978.
[21] J. H. Kim, "Thrust-vector control based terminal guidance law using convex programming," Ph.D. dissertation, College Eng. Sci., Inha Univ., Incheon, South Korea, 2021.
[22] Missile Defense Advocacy Alliance, "Network centric airborne defense element (NCADE)," Accessed on: Jan. 25, 2023. [Online]. Available: https://missiledefenseadvocacy.org/defense-systems/network-centric-airborne-defense-element-ncade/
[23] C. C. Rosema, J. B. Doyle, and W. B. Blake, "Missile data compendium (DATCOM) user manual 2014 revision," Accessed on: Jun. 5, 2023. [Online]. Available: https://apps.dtic.mil/sti/citations/AD1000581

Ha-Min Jeon received the B.S. degree in aerospace engineering in 2020 from Inha University, Incheon, South Korea, where he is currently working toward the Ph.D. degree in high-altitude terminal guidance and control with the Department of Aerospace Engineering.

His recent research areas include the guidance and control system for missiles and reusable launch vehicles, trajectory optimization, and fault classification and detection for engine rotor.

Tae Young Kang received the B.S. degree in aerospace engineering in 2018 from Inha University, Incheon, South Korea, where he is currently working toward the Ph.D. degree in optimal guidance with the Department of Aerospace Engineering.

His recent research areas include the guidance and control system for missiles and unmanned aerial vehicles (UAVs), and trajectory optimization and path planning for UAVs.

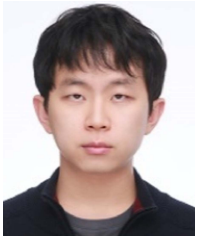

Jongho Park received the B.S., M.S., and Ph.D. degrees in aerospace engineering from the Department of Mechanical and Aerospace Engineering, Seoul National University, Seoul, South Korea, in 2010, 2012, and 2016, respectively.

From 2016 to 2019, he was a Senior Researcher for the Guidance and Control Team with the Agency for Defense Development, Daejeon, South Korea. In 2019, he joined the faculty of Ajou University, Suwon, South Korea, where he is currently an Assistant Professor with the Department of Military Digital Convergence and the Department of AI Convergence Network. His research interests include guidance, control, and applications of aerospace systems.

Chang-Kyung Ryoo received the B.S. degree from Inha University, Incheon, South Korea, in 1989, and the M.S. and Ph.D. degrees from the Korea Advanced Institute of Science and Technology, Daejeon, South Korea, in 1991 and 2006, respectively, all in aerospace engineering.

From 1991 to 2006, he was a Research Engineer with the Agency for Defense Development, South Korea. He is currently a Professor with the Department of Aerospace Engineering, Inha University. His recent research areas are guidance and control system for missiles and unmanned aerial vehicles, nonlinear systems control, and trajectory optimization.